Non-destructive vacuum-assisted measurement of lung elastic modulus

Jiawen Chen[a,1], **Seyed Mohammad Mir**[a,1], **Meghan R. Pinezich**[b], **John D. O'Neill**[c], **Brandon A. Guenthart**[d], **Matthew Bacchetta**[e], **Gordana Vunjak-Novakovic**[b], **Sarah X.L. Huang**[f], **Jinho Kim**[a,*]

[a] Department of Biomedical Engineering, Stevens Institute of Technology, Hoboken, NJ, United States

[b] Department of Biomedical Engineering, Columbia University, New York, NY, United States

[c] Department of Cell Biology, State University of New York Downstate Medical Center, Brooklyn, NY, United States

[d] Department of Cardiothoracic Surgery, Stanford University, Stanford, CA, United States

[e] Department of Thoracic Surgery, Vanderbilt University, Nashville, TN, United States

[f] Center for Stem Cell and Regenerative Medicine, University of Texas Health Science Center, Houston, TX, United States

Abstract

In living tissues, mechanical stiffness and biological function are intrinsically linked. Alterations in the stiffness of tissues can induce pathological interactions that affect cellular activity and tissue function. Underlying connections between tissue stiffness and disease highlights the importance of accurate quantitative characterizations of soft tissue mechanics, which can improve our understanding of disease and inform therapeutic development. In particular, accurate measurement of lung mechanical properties has been especially challenging due to the anatomical and mechanobiological complexities of the lung. Discrepancies between measured mechanical properties of dissected lung tissue samples and intact lung tissues in vivo has limited the ability to accurately characterize integral lung mechanics. Here, we report a non-destructive vacuum-assisted method to evaluate mechanical properties of soft biomaterials, including intact tissues and hydrogels. Using this approach, we measured elastic moduli of rat lung tissue that varied depending on stress-strain distribution throughout the lung. We also observed that the elastic moduli of enzymatically disrupted lung parenchyma increased by at least 64%. The reported methodology enables assessment of the nonlinear viscoelastic characteristics of intact lungs under

*Corresponding author. jkim6@stevens.edu (J. Kim).
[1]These authors contributed equally to this work.

normal and abnormal (i.e., injured, diseased) conditions and allows measurement of mechanical properties of tissue-mimetic biomaterials for use in therapeutics or in vitro models.

Keywords

1. Introduction

Stiffness is a fundamental property of living tissues that influences cellular activity and supports tissue function. Defined as the extent to which a material resists deformation in response to an applied force [1–3], stiffness is represented by elastic modulus (E). Tissue stiffness is determined by the tissue-specific profile and assembly of extracellular matrix (ECM) components, and E ranges from ~10^3 Pa (brain, fat) to ~10^9 Pa (bone) in human [4,5]. Alterations in tissue stiffness can cause impaired reciprocal interactions between cells and their environment that can lead to dysregulated cellular behaviors and tissue function [5–8]. For example, the pathological ECM remodeling associated with fibrotic diseases such as pulmonary fibrosis, liver cirrhosis, and scleroderma can significantly alter tissue mechanics [9–11]. The strong association between tissue stiffness and disease highlights the need for accurate quantitative evaluation of the mechanical properties of tissues, and represents a significant opportunity to improve our understanding of disease and develop new therapeutics [12].

Techniques that are typically used to assess tissue stiffness include tensile testing, micro-/nano-indentation, or atomic force microscopy (AFM) [13–15], but involve destructive methods that require dissection of tissue samples from the organ to measure mechanical properties. Tissue removal from the lung is especially detrimental to the accuracy of mechanical analyses because lung mechanics are determined by the complex structures, hierarchical branching, and exquisite biochemical organization of the lung in situ, features that may be compromised or lost during conventional assessments. The gas exchange region of the lung is highly vascularized and aerated, containing nearly 500 million air sacs (i.e., alveoli), each approximately 200 – 300 μm in diameter. The surface of alveoli is lined with a thin layer of fluid called pulmonary surfactant secreted by alveolar type II cells that increases lung compliance (i.e., elasticity) by reducing the surface tension in the alveoli [16,17]. Lung compliance can be substantially reduced in lung injury, such as in acute respiratory distress syndrome (ARDS), due to accumulation of protein-rich fluids in the alveoli that disrupt the surfactant layer [18,19]. In lung fibrosis, elastic fibers are replaced by collagens, which leads to increased lung stiffness (i.e., decreased lung compliance) [20,21]. While accurate characterization of lung tissue mechanics can facilitate therapeutic development, the complex biophysical features that govern the viscoelastic characteristics of the lung can be substantially altered in parenchymal tissue samples isolated from the lung for assessment [15,22]. Thus, use of existing methods to determine the mechanical properties of lung tissues may not fully capture the complex mechanical characteristics and dynamic behaviors of the intact lung, underscoring the critical need for non-destructive approaches for lung tissue characterization.

Innovative methodologies have been developed for quantification of mechanical properties of tissues or organs in a non-destructive manner. For example, imaging modalities, including ultrasound, optical coherent tomography (OCT), and magnetic resonance imaging (MRI), have been utilized to estimate tissue stiffness by imaging tissue displacement in response to mechanical force [23] or by measuring speed of shear waves propagating through the tissue [24,25]. These methods enabled qualitative or quantitative assessment of elastic properties of tissues to diagnose and characterize different diseases, such as cancer, fibrosis, and inflammation [26,27]. Because these imaging-enabled approaches require expensive, complex, and bulky imaging systems, there have been efforts to establish simpler methods that can allow non-destructive tissue characterization with reduced cost and system complexity. In particular, compression test has been used to determine tension of the visceral pleural membrane and Young's modulus of the lung by correlating tissue deformation and uniaxial compressive load [28–30]. Further, viscoelastic mechanical response of tissues, including skin and liver tissue, have been determined by evaluating elongation of local tissue in response to applied vacuum pressure [31,32]. Notably, the vacuum-based methods have been extensively used to study micromechanics of cell membrane as the method is capable of inducing gentle deformation of the cell without damaging its delicate structure [33,34].

In this research article, we explore the utility of the vacuum-assisted modality for accurate non-destructive measurement of the elastic moduli of soft biological materials, such as hydrogels and lung. We constructed an integrated measurement platform with computer-controlled sensors, custom-built microscope, and negative pressure generator that enabled accurate, non-destructive measurements of the stiffness of lung tissue. We tested this system using gelatin hydrogels of variable stiffness and explanted rat lungs (Fig. 1), and verified measurement accuracy and reproducibility by comparison with values reported in the literature. Notably, our approach allowed rapid and precise determination of the elastic modulus of enzymatically disrupted lung without removal of tissue from the lungs. This methodology can be used to expand our knowledge about the correlation between biophysical properties of the lung and different respiratory disorders.

2. Materials and methods

2.1. Preparation of crosslinked gelatin hydrogels

Gelatin hydrogels (4, 10, 15% w/v) were prepared by dissolving gelatin powder (G2500, Sigma-Aldrich) into deionized water at 70°C. To improve visibility of the hydrogel boundary for accurate assessment of gel deformation with our imaging system, we added 20 μL of fluorescein (1 mg/mL; excitation/emission: 498 nm/517 nm; F6377, Sigma-Aldrich) to 4 mL of molten gelatin solution. Aerated hydrogels were produced by vortexing the molten gel solution manually using a metal mixing rod to create micro-air bubbles within the solution for approximately 5 min while gelation was occurring. Further, hydrogels embedded with fluorescent microparticles (diameter: 10 μm, excitation/emission: 505 nm/515 nm; F8836, Invitrogen) were prepared by adding 3 μL of the particle solution into 4 mL of molten gel solution (final particle concentration: ~3000 particles/mL). To generate gelatin hydrogels for measurements, 30 μL of molten gelatin solution was placed on a

polydimethylsiloxane (PDMS) substrate. The hydrophobic PDMS facilitated formation of dome-shaped gelation hydrogels which gelled after 10 min at 4°C.

2.2. Explant of rat lungs

Lungs ($n = 6$) were explanted from Sprague-Dawley rats (equal numbers of males and females; 200 – 250 g; SAS SD Rats, Charles River Laboratories) and used for lung tissue stiffness measurements. All procedures were performed in accordance with the animal welfare guidelines and regulations of the Institute for Animal Care and Use Committee (IACUC) at Stevens Institute of Technology. Prior to lung explant, animals were euthanized with 5% Isoflurane (VED1350, Penn Veterinary Supply) for 30 min using a vaporizer (SomnoSuite, Kent Scientific). At time of explant, the chest was opened using a surgical scalpel and scissors. An endotracheal cannula (73–2727, Harvard Apparatus) was inserted into the trachea and secured using a 6–0 prolene suture (Ethicon). Cannulated lungs were kept intact and carefully removed from the chest. The endotracheal cannula was connected to a small animal ventilator (PhysioSuite, Kent Scientific) and ventilated with tidal volume of 6 mL/kg at rate of 30 breath per minute (bpm). During ventilation, pressures and volumes were monitored through an integrated sensor in the ventilator. To eliminate variation between the lungs that could be caused by inflation and deflation history, we ventilated all the lungs for 5 min prior to the stiffness measurements. In this study, the lungs were not perfused.

2.3. Disruption of rat lung parenchyma

To induce tissue disruption in isolated rat lungs, trypsin solution (concentration: 0.25%; volume: 1 mL) was instilled through the trachea of freshly explanted rat lungs while the lungs were positioned in the prone position. To visually confirm delivery of the solution in the lung parenchyma in real time, indocyanine green fluorescent dye (ICG; Cardiogreen, Sigma-Aldrich Inc.; excitation/emission: 785 nm/820 nm) was mixed in the trypsin solution prior to the administration. A custom-built near-infrared imaging system was used to visualize distribution of the trypsin/ICG solution throughout the lung. Before stiffness measurements, the trypsinized lungs were continuously ventilated for 10 min to induce enzymatically induced damage in the alveolar spaces. Accumulation of edematous fluid, disruption of alveolar cell membrane, and depletion of surfactant layer in the alveolar space were visually confirmed via histology.

2.4. Histology

All lungs were fixed by immersion in 4% paraformaldehyde (30,525–89–4, Acros Organics) for 48 h at 4°C. Lungs were inflated with air (volume: ~10 mL), and the trachea was clamped to ensure the lung remained open during fixation. The fixed lungs were then dehydrated using ethanol (70% – 100% v/v) and CitriSolv (1601, Decon Laboratories), embedded in paraffin, sectioned at 5 μm thickness, and mounted on glass slides. Prior to staining, lung sections were de-paraffinized in CitriSolv and rehydrated in ethanol and water. Tissue sections were stained with hematoxylin and eosin (H&E) according to the manufacturer's instructions (ab245880, Ab-cam).

2.5. Vacuum-assisted stiffness measurement system

The vacuum-based stiffness measurement system was constructed by integrating: glass capillary, pressure sensor, programmable syringe pump, light sources, custom-built microscopic imaging system, micro-manipulator, and computer. A thin capillary (inner diameter: 0.58 mm, outer diameter: 1 mm, length: 76 mm; 1B100F, World Precision Instruments) was used for gelatin hydrogels, and a thick capillary (inner diameter: 1.5 mm, outer diameter: 1.8 mm; CV1518–300, VitroCom) was used for lungs. The capillary was connected to a 5-mL syringe via polymer tubing, and the syringe was loaded in a programmable syringe pump (AL-4000, World Precision Instruments). Air pressure was monitored using a pressure sensor (pressure range: ±25 kPa; MPXV7025GC6U-ND, NXP USA) and a digital data acquisition device (Arduino Uno) controlled with custom-written MATLAB code (MathWorks). The glass capillary was attached to a micro-manipulator (PT3, Thorlabs) that enabled precise manipulation of the capillary position to achieve gentle contact without damage to delicate hydrogels or lung tissues. To eliminate potential measurement variation across different lungs, including both healthy and defective lungs, we measured the modulus at a similar anatomical location (i.e., right middle lobe).

2.6. Whole lung compliance measurements

To measure whole lung compliance, we constructed a sensing model that can measure airway pressure (P_{Alv}) and lung volume (V) during ventilation. The system consists of a pressure sensor (pressure range: ±7 kPa; MPXV7007GC6U, NXP), airflow sensor (flow range: ±750 cm^3/min, HAFBLF0200CAAX5, Honeywell), and digital signal acquisition device (Arduino Uno). The pressure–volume sensor module was connected between the ventilator and endotracheal cannula to record and process signals using a custom-written MATLAB code.

2.7. Fluorescence microscopy

To monitor the deformation of hydrogels or tissues within the glass capillary, we constructed a custom-built fluorescence microscope comprised of an objective lens (RMS10X, Olympus), scientific CMOS camera (Manta G-145 NIR, Allied Vision), and light sources (MWWHLP1 LED, Thorlabs; MDL-D-488 Laser, OptoEngine). A white LED light source was used to illuminate samples during brightfield imaging, and a 488-nm laser was used to visualize fluorescein (excitation/emission: 460 nm/515 nm; F6377, Sigma-Aldrich) mixed in gelatin hydrogels or labeled in lung pleural tissue, which enhanced visibility of the hydrogel and lung tissue boundary during measurement and analysis. The laser was transmitted from the laser generator through an optical fiber bundle (MHP910L02, Thorlabs) and focused on samples via an achromatic lens (AC254–100-AB-ML, Thorlabs). Laser power was adjusted to obtain optimal fluorescence signals, which were passed through an emission filter (ET535/50 m, Chroma) and focused onto the image sensor of the camera via a tube lens (AC254–75-AB-ML, Thorlabs). Images and videos were recorded using image acquisition software (Vimba, Allied Vision).

2.8. Near-infrared imaging of whole lungs

To visualize distribution of the trypsin/ICG solution, we constructed a near infrared (NIR) imaging system that enabled noninvasive detection of ICG fluorescence signal by imaging through the lung pleura [35–38]. The NIR imaging system consisted of a scientific CMOS camera (Manta G-145 NIR, Allied Vision), camera lens (50 mm C-Series VIS-NIR lens, Edmund Optics), 785-nm laser (MDL-III-785, OptoEngine), and NIR filter set (ICG-B-000, Semrock). Laser power, camera lens focus and aperture, and exposure time were adjusted to obtain optimal NIR images.

2.9. Stiffness calculation via image processing and analysis

All image processing, analysis, and reconstruction was performed using ImageJ software (NIH). The brightness and contrast of all images and image frames extracted from videos of the same experimental group were adjusted identically. To process videos using ImageJ software, all videos were converted into AVI files and compressed using MJPEG compression format. A video file was imported into ImageJ as an image sequence for further image processing and analysis. The boundary of gelatin or lung tissue in an image was determined using the "edge detection" function, in which a thin line at the interface between the sample (gray) and background (black) was identified based on pixel intensity and plotted as a gray image. Edge images obtained at different times were combined into a single image using the "image calculator" function to show time-dependent deformation. To visualize fluctuation of a selected region over time in a single image, we used the "image stitching" method, in which a selected spot at the edge of the sample (e.g., region with maximum deflection) was extracted from each image frame of an image sequence. The extracted region of interest (ROI) in each frame was stitched along the horizontal direction to show change of the elongation of the ROI over time. Elastic modulus (E) was then computed by $E = 3CR_PP_V/2\pi L_E$, where C is a constant specific to the geometry of the capillary used to apply vacuum pressure, R_P is radius of the capillary used for measurement, P_V is vacuum pressure, and L_E is sample elongation length. For a tubular capillary, C is ~2.1 [39–42].

2.10. Statistical tests

All data were obtained from experiments repeated at least three times and are reported as mean ± standard deviation. One-way analysis of variance (ANOVA) was used to determine statistically significant differences between groups, with $p < 0.05$ considered significant.

3. Results

3.1. Measurement and calculation of elastic moduli of gelatin hydrogels

We constructed an integrated system that can non-destructively measure the elastic modulus of soft biomaterials (e.g., hydrogels; Fig. 1A) and soft tissues (e.g., lung; Fig. 1B). The system can generate and dynamically apply a range of set values of vacuum pressure (P_V) to the surface of a biomaterial or tissue via glass capillary connected to a programmable syringe pump. The glass capillary probe is precisely controlled by a micromanipulator. As vacuum pressure is applied, the surface of the test sample is deformed. To determine elastic modulus, deformation is monitored using a custom-built microscope (Fig. 1C–D).

To evaluate system functionality and measurement accuracy, we formed gelatin hydrogels (4% w/v) on a PDMS substrate (Fig. 2). Gelatin hydrogels were labeled with fluorescent dye to improve visibility of the gel boundary during deformation (Fig. 2A). After a glass capillary probe (inner diameter: 0.58 mm) was placed in gentle contact with the upper surface of a gelatin hydrogel, vacuum pressure (P_V) was gradually changed from 0 to -8.2 kPa at a rate of -2.25 kPa/s within 3.6 s. As negative pressure continued to increase, the region of gelatin subjected to vacuum pressure was gradually elongated inside the capillary tube (Fig. 2A). To quantify gel deformation, we used ImageJ to extract the edge of the gel at different time points (Fig. 2B). Then, the edge of the hydrogel with greatest deformation, i.e., the region subjected to negative pressure, was cropped from each image and merged into a single composite image (Fig. 2C), enabling visualization of hydrogel deformation over time.

We evaluated the stiffnesses of gelatin hydrogels with different concentrations (4, 10, 15% w/v; Fig. 3; Supplementary Videos 1–3). Vacuum pressure (P_V) and elongation length (L_E) were measured and plotted for (*i*) 4% (Fig. 3A), (*ii*) 10% (Fig. 3B), and (*iii*) 15% w/v (Fig. 3C) gelatin hydrogels. In all experiments, the rate of increased or decreased pressure (i.e., slope of pressure curve) during measurement was 2.25 kPa/s. Furthermore, the maximum elongation length of gelatin, which corresponded with the center of the deflected region, was plotted against time via edge detection, feature extraction, and image stitching using ImageJ. Maximum elongation lengths were 0.115 mm for 4% w/v gelatin with P_V of -8.2 kPa, 0.034 mm for 10% w/v gelatin with P_V of -11.8 kPa, and 0.022 mm for 15% w/v gelatin with P_V of -14.8 kPa.

We then compared the stretched length (L_E) of the three different hydrogels during elongation and relaxation periods when the negative pressure was -5 kPa (Fig. 3D). No significant differences in L_E were observed between stretching and relaxation in gelatin hydrogels of the same concentration. For example, L_E of 4% gelatin measured during elongation (0.13 ± 0.04 mm) and relaxation (0.13 ± 0.02 mm) showed no significant difference ($p = 0.825$). However, the average elongation of 4% w/v gelatin (0.13 ± 0.03 mm) was significantly greater than those of 10% w/v gelatin (0.046 ± 0.01 mm, $p < 0.001$) and 15% w/v gelatin (0.03 ± 0.01 mm, $p < 0.001$) under P_V of -5 kPa (Fig. 3D). Using the measured values, we computed the elastic modulus (E) of each gelatin hydrogel. For 4, 10, and 15% w/v gelatins, E were 11.4 ± 2.3, 31.5 ± 6.7, and 49.8 ± 13.0 kPa, respectively (Fig. 3E). The results are consistent with the elastic modulus values measured via compression test (Supplementary Fig. 1) and the range of published values obtained through various conventional measurement methods [43–45] (Supplementary Table 1). Comparisons of moduli between different gelatin groups (e.g., 4% vs 10%, 4% vs 10%, etc.) indicated significant correlation between E and gelatin concentration ($p < 0.001$). Notably, inner diameter of the capillary probe (D_I) was proportional to the depth of the negative pressure energy propagates within the gel (Supplementary Fig. 2). In particular, larger probe ($D_I = 1.5$ mm) can elongate and therefore, measure stiffness of deeper regions of hydrogel compared to thinner probe ($D_I = 0.58$ mm) which provides more superficial measurements.

3.2. Effects of porosity on stiffness of gelatin hydrogels

We investigated whether the elastic modulus of an aerated hydrogel can be also measured using our measurement setup and approach without damaging its delicate porous structure (Fig. 4; Supplementary Video 4). Aerated 10% w/v gelatin was prepared and evaluated mechanically in comparison with non-aerated 10% w/v gelatin (control). Aerated gels were created by blending air into the gelatin during gelatin, resulting in the generation of microbubbles (diameter: ~200 μm) within the gel (Fig. 4A). Similar to the experiments with non-aerated gels (Fig. 3), vacuum pressure between 0 kPa and −10 kPa was applied to the gel while the shape deformation was recorded for post-analysis (Fig. 4B). Elongation of the aerated gel during three cycles of stretching and relaxation was determined via the recorded videos and plotted with the control gel. In this study, the maximum deflection measured was ~0.145 mm and 0.082 mm for the aerated gel and non-aerated gel, respectively (Fig. 4C). Based on the deformation mechanics, the elastic modulus of the aerated 10% w/v gelatin was determined to be 15.1 ± 5.4 kPa, which was significantly lower ($p < 0.001$) than that of the non-aerated gelatin (31.5 ± 6.7 kPa; Fig. 4D).

3.3. Non-destructive measurement of elastic modulus of rat lungs

We used intact rat lungs to investigate whether the elastic modulus of lung tissue can be measured non-destructively using the vacuum-assisted method (Fig. 5; Supplementary Videos 5–7). During measurements, the intra-alveolar pressure of the lung (P_{Alv}) was maintained at a constant level (2, 5, 10 cmH$_2$O) without ventilating lungs to minimize motion-induced measurement error and prevent tissue damage that could be caused by uncontrolled contact of the capillary probe with the tissue surface. To improve visualization of tissue deformation, a 488-nm laser was used to directly illuminate the lung pleural tissue labeled with fluoresceine molecules prior to measurements (Fig. 5A, i). The pressure inside the lung (P_{Alv}) was controlled and monitored using a syringe connected to a pressure sensor (Fig. 5A, ii). Photographs showed deformation of lung tissue under a negative pressure (P_{V}) of −2 kPa via a capillary tube (inner diameter: 1.5 mm) while different P_{Alv} (2, 5, 10 cm H$_2$O) were maintained within the lung (Fig. 5B). Further, we measured the elongation length of the lung tissue (L_{E}), while P_{V} was increased and decreased to imitate the stress-strain (i.e., pressure-volume) measurements of lung (Fig. 5C; Supplementary Fig. 3). Measured L_{E} varied nonlinearly in response to P_{V} while the loading-unloading curve exhibited hysteresis which is a unique behavior of viscoelastic materials, including lung tissue. In addition, we measured L_{E} while varying rate of change of vacuum pressure magnitude ($|P_{\mathrm{V}}|$) (i.e., 2 kPa/s, 0.66 kPa/s, and 0.2 kPa/s) (Supplementary Fig. 4). Notably, increased rate change of $|P\mathrm{V}|$ resulted in reduced L_{E} indicating viscoelastic deformation pattern of the lung. We further confirmed the non-linear deformation of lung tissue by measuring L_{E} while increasing $|P_{\mathrm{V}}|$ from 0.7 to 10 kPa in a step-wise manner (Supplementary Fig. 5). At lower pressure ($|P_{\mathrm{V}}| < 2$ kPa), L_{E} increased rapidly with $|P_{\mathrm{V}}|$ while further increasing magnitude of the negative pressure (e.g., $|P\mathrm{V}| > 5$ kPa) resulted in decreased rate of tissue elongation, highlighting non-linear correlation between L_{E} and $|P_{\mathrm{V}}|$.

Notably, as pressure inside the lung increased, L_{E} decreased. For P_{Alv} of 2, 5, and 10 cmH$_2$O, L_{E} were 0.33 ± 0.05, 0.20 ± 0.03, and 0.12 ± 0.03 mm (Fig. 5D), and E were 4.4 ± 0.6, 7.4 ± 1.1, and 13.2 ± 3.9 kPa, respectively (Fig. 5E). The results indicate that there was

an interaction between P_{Alv} and E (0.2 vs 0.5 kPa: $p = 0.005$; 0.2 vs 1.0 kPa: $p = 0.0058$; 0.5 vs 1.0 kPa: $p = 0.067$). Such alveolar pressure dependence is due to the changes in tension (T) within the pleural layer and alveolar septal network with respect to the air pressure inside. As the lung volume increases, the collagen fibrils in the tissue become stress-bearing while their waviness is lost, leading to increased tissue elastic modulus [46]. Therefore, as the internal pressure of the lung elevates by increasing the volume of air in the lung, tension in the lung tissue also increases, requiring a greater vacuum pressure to stretch the lung tissue against the resisting tensile force [47,48] (Supplementary Fig. 6). Lung stiffness measured using the vacuum-based method were within ranges reported in the literature, obtained using a broad range of mechanical testing methods, including indentation, atomic force microscopy, and tensile testing (Supplementary Table 2).

3.4. Alterations in stiffness caused by alveolar disruption

We further investigated whether changes in the stiffness of lung parenchymal tissue caused by enzymatic disruption can be detected using our approach. To induce acute tissue disruption, the lung was exposed to an enzymatic solution (i.e., trypsin) that can dislodge epithelial cells from ECM and further disrupt the surface tension in the alveolar space (Fig. 6; Supplementary Videos 8–9) [49]. The goal of trypsinization was not to mimic stereotypical presentation of any one pathology, but rather to assess the ability of the vacuum-assisted method to quantify changes in lung tissue stiffness [50,51]. The rat lung was instilled with 0.25% trypsin (1 mL) with ICG dye through the trachea and incubated for 10 min. Distribution of the trypsin solution within the respiratory tract of the lung was confirmed through visualization of trypsin/ICG via NIR imaging of the lung (Fig. 6B, i–ii). We monitored static compliance (C_S) of the whole lung before and after the trypsin challenge by measuring its pressure–volume relation, where air pressure (P_{Alv}) and lung volume (V) were measured using our custom-built sensor module. Static compliance (C_S) was calculated by $C_S = \mathrm{TV}/(P_{Plat} - \mathrm{PEEP})$, where TV is tidal volume, P_{Plat} is plateau pressure, and PEEP is positive end-expiratory pressure. While the healthy lungs (control) displayed high static compliance (0.70 mL/cmH$_2$O), damaged lungs showed substantially reduced compliance (0.29 mL/cmH$_2$O), as trypsinized lungs required significantly greater pressures when ventilated with the same air volume (Fig. 6C). Histological analysis via H&E staining of the trypsinized lung showed excessive accumulation of fluid and debris in alveolar spaces with substantial reduction of intact cells and decreased number of nuclei compared to control lungs (Fig. 6D, i & ii; supplementary Figs. 7 & 8). In the trypsinized lungs, maximum elongation lengths under P_V of −2 kPa were 0.11 ± 0.01 and 0.07 ± 0.01 mm, respectively, for 5 and 10 cmH$_2$O of P_{Alv} (Fig. 7A). As a result, elastic moduli of the enzymatically damaged lungs were determined to be 12.8 ± 1.0 and 21.7 ± 3.9 kPa, respectively, for 5 and 10 cmH$_2$O of P_{Alv}, indicating 73.1% and 64.6% increases in tissue stiffness compared to the control (healthy) lungs under the same measurement conditions (Fig. 7B). The significant increase in E following proteolytic tissue disruption, in particular for P_{Alv} of 5 cmH$_2$O ($p = 0.003$), suggests that the intrinsic deformation mechanics and stiffness of the lung tissue parenchyma was compromised following trypsin challenge. Further, in the damaged lungs the effects of P_{Alv} on E were considerable ($p = 0.02$), highlighting the influence of measurement conditions such as intraalveolar pressure on tissue characterization. Notably, no physical damages to the lung parenchyma or pleura (e.g.,

blistering or rupturing) were observed in the visceral pleural layer of the lungs following the vacuum-based measurements (Supplementary Fig. 9).

4. Discussion

Here, we report a non-destructive vacuum-assisted method to measure elastic moduli of soft tissues and biomaterials. This method allows for stiffness measurement in a non-destructive, localized, and rapid manner. The enabling underlying principles of this method are that: (*i*) soft tissues and biomaterials can deform when subjected to gentle vacuum pressure, and (*ii*) degree of deformation depends on the stiffness of the material. Although methods exist for assessing the stiffness of soft tissues and biomaterials (e.g., rheometry, tensile testing, micro-/nano-indentation, atomic force microscopy), these methods typically require destructive lung tissue preparation procedures (e.g., biopsy and tissue slicing) [39,52,53]. Thus, these methods cannot be readily applied to intact lungs and lack translational potential for integration into medical devices for assessing tissue stiffness – a fundamental property of living tissues that can offer diagnostic and/or prognostic insights. While compression-based or indentation techniques have been used to assess mechanical properties of explanted lungs without tissue dissection [28–30], the equipment currently required for such systems (i.e., rigid probes and bulky stress/strain sensors) preclude their incorporation into minimally invasive and flexible devices capable of measuring tissue stiffness in situ. On the other hand, our vacuum-based system could be modified into an integrated, portable, steerable, and miniaturized device to allow localized in situ assessment. For example, the glass tube used in current study can be replaced with a flexible, transparent polymer tubing and combined with a steerable endoscope to quantify local tissue stiffness not only within thorax but also in other organs and tissues, including cardiovascular or gastrointestinal tissues.

We first tested our vacuum-based stiffness measurement method using gelatin hydrogels of various concentrations (4, 10, 15% w/v), and measured mean elastic moduli between 11.4 ± 2.3 and 49.8 ± 13.0 kPa, consistent with reported values [43–45]. To determine the feasibility of evaluating tissue-mimetic materials, we prepared an aerated gel with pores (~200 μm) designed to mimic the alveolar architecture of the lung. We used our method to measure stiffness of the porous 10% w/v gelatin hydrogel, and determined that elastic modulus (average: 15.1 ± 5.4 kPa) was nearly 50% lower than the elastic modulus of non-aerated 10% w/v gelatin (average value: 31.5 ± 6.7 kPa), indicating that the aerated structure of the porous gel increased elasticity (i.e., decreased stiffness) under vacuum loading. This application demonstrates the utility of our method in evaluation of tissue-mimetic delicate materials.

We then applied our method to evaluate the stiffness of intact lung tissues. Lung tissue was labeled with fluorescein to more easily visualize the boundary of the lung during measurements, allowing accurate evaluation of tissue deformation across conditions. Notably, the lungs displayed nonlinear viscoelastic deformation behaviors. Further, average values of tissue elongation decreased as the pressure inside the lung increased from 2 to 10 cmH$_2$O, corresponding to measured lung elastic moduli of $\sim 4.4 \pm 0.6$ and 13.2 ± 3.9 kPa, respectively, for P_V of -2 kPa. The increase in tissue stiffness with respect to P_{Alv} could be due to increased tension throughout the tissue region, which limited tissue deformation.

The resistance of the lung tissue to deform resulted in reduced tissue elongation for a specific vacuum pressure applied to the tissue surface. Specifically, to elongate lung tissue under tension to the same degree as lung tissue without tension, a higher vacuum pressure would be required, leading to an increased elastic modulus calculated for the pre-stretched lung tissue [54–56]. This result underscores the importance of measuring lung mechanical properties under conditions that closely resemble the *in-vivo* environment (e.g., intact lung structure, physiological airway pressure and volume). Since P_{Alv} of the intact lungs measured during positive pressure ventilation can vary during the breathing cycle (~5–40 cm H_2O in human) [57,58], physiologically-relevant pressure ranges should be maintained within the lungs during measurement for accurate evaluation of lung tissue stiffness. Further, while the exact physiologic preload throughout the lung is difficult to determine [59,60], P_{Alv} can be used to represent the stress-strain state of the lung in vivo condition.

The vacuum-based method can allow accurate measurement of lung tissue without altering its intrinsic structure, anatomy, or biology. The elastic moduli measured using this method, however, reflect the stiffness of lung tissue resulted from interplay between the visceral pleural layer, alveolar septal network, and the alveolar surface tension at the measurement site. Notably, the role of the visceral pleural tissue will become increasingly important when this method is applied to large species, such as human and swine, because of their thicker and more complex pleural tissue structure. In rat lungs, however, the pleura is notably thin and elastic (< 10 μm [61]) and thus the tissue stiffness measured can be predominantly determined by the alveolar architecture and surface tension force. This is evidenced by our experimental results that showed substantial increase (> 64.6%) in the lung tissue stiffness following a trypsin challenge of the alveolar space. If the mechanical properties of the visceral pleura dominated the measurements, the stiffness between the healthy and disrupted lungs would be nearly the same. Further, it is expected that the stiffness of perfused lung would be greater than non-perfused lung because elevated perfusion pressure within the blood vessel network due to circulation of blood or blood-like medium can contribute to increased lung tissue stiffness [62].

We also hypothesized that a non-destructive method for measuring tissue stiffness could potentially be used to assess changes in lung mechanics that occur due to injury or disease. To test this hypothesis, we disrupted the alveolar tissue via intratracheal instillation of trypsin solution and measured the resulting change in lung stiffness. Intratracheal delivery of trypsin into the rat lung led to increased stiffness of the disrupted lung tissue. Specifically, elastic moduli of trypsinized lungs determined under P_V of −2 kPa were ~12.8 ± 1.0 and 21.7 ± 3.9 kPa, respectively, for 5 and 10 cmH_2O of P_{Alv}, which represent 73.1 and 64.6% increases in tissue stiffness compared to control lungs. Underlying mechanisms that contributed to the increased stiffness include: (*i*) displacement or dilution of pulmonary surfactant in the alveoli leading to increased alveolar surface tension and decreased compliance [63–65] and (*ii*) detachment of native cells from the airway basement membrane, leading to loss of barrier function, development of pulmonary edema (fluid accumulation in the airways and interstitium), and reduced elasticity [66,67]. We observed the correlation between the elastic moduli and lung compliances determined in both healthy and disrupted lungs. Increase in the elastic moduli of trypsin-challenged lungs were reflected by decreased lung compliance determined via pressure-volume relation measurements. The

tissue disruption induced by trypsinization can be irrelevant to the injury patterns typically seen in human ALI or ARDS [50,51]. Nevertheless, the measurement results demonstrate that the vacuum-based method is capable of quantifying alteration of the mechanical properties in the enzymatically disrupted lung parenchyma. Stiffness measured at different locations of healthy and trypsinized lungs can offer invaluable information of the relation between tissue quality and function. However, because main objective of this study is to quantify the difference between healthy and damaged lungs, we measured the stiffness at an anatomically similar location of the lungs (i.e., right middle lobe) regardless of the injury state of the tissue region.

The results collectively indicate that our non-destructive, vacuum-based lung tissue stiffness measurement method could accurately quantify and predict the lung tissue mechanics and behaviors compared to destructive methods, and may be appropriate for evaluations both *ex vivo* and in vivo. Pressure and volume (P-V) measurements will continue to offer valuable clinical information regarding compliance and stiffness of global lung (i.e., the average of both lungs). The vacuum-assisted method, while more invasive, can provide information that is site and tissue specific and could be used to identify changes in each lung, lobe, or segment, providing regional insight and information. While this may be useful in intubated patients, we envision it has much more clinical and translational potential in other applications, such as utilizing our method at the time of surgery (whether its open or thoracoscopic/robotic approaches), during *ex vivo* lung perfusion (donor lung assessment and reconditioning), and as a tool to aid in lung bioengineering. For example, donor lungs that are initially unsuitable for transplantation, often due to acute injury and edema, can sometimes be recovered using *ex vivo* machine perfusion. Our non-invasive method for measuring stiffness could be used to assess edema or acute tissue injury in donor lungs to aid in determination of suitability for transplantation, including in lungs recovering on *ex vivo* perfusion systems [36,38].

Additionally, solid tumors often display differential mechanical properties from the surrounding tissue [68,69]. A major challenge of tumor resection is difficulty identifying the boundaries of the tumor, ensuring that all tumor tissue is removed while minimizing removal of normal tissue [70]. A non-destructive mechanical testing method similar to those described here could also be used intraoperatively during surgery to determine tumor margins (e.g., tumors located in the lung periphery) in real-time with high spatial resolution and facilitate reliably effective tumor resection. Measurement number and duration would largely depend on the properties of the tumor, such as stiffness, size, and location. Additionally, we envision future integration and use in conjunction with other imaging modalities for localization and diagnostic purposes. Further research and refinement of our methodology may also be useful in distinguishing lung pathology which is often clinically difficult to distinguish without tissue biopsy (e.g., atelectasis vs infiltrate, tumor vs granuloma, consolidation vs fibrosis etc.).

Despite the advantages, the vacuum-based method has several limitations. During the experiments, we observed surface desiccation of lung tissues and hydrogels, which can cause increased stiffness over time. The tendency for samples to dehydrate may be more significant for tissues and biomaterials that contain high water content. One technique for

overcoming this limitation would be to maintain ambient humidity at 100% to prevent dehydration during testing [71,72]. During image analysis to determine sample deformation, we occasionally observed irregularity in the sample edge. Such irregularity was mainly caused by low quality of images obtained during measurement. To reduce the measurement uncertainty, an objective lens with higher magnification or adjustments to imaging angle could be used to improve image quality and resolution for more accurate edge detection. Further, while explanted rat lungs were used in this study, the role of the chest cavity on lung stiffness can be considerable. It is because measured stiffness depends on the stress-strain distribution throughout the lung and can be affected by the surrounding air pressure and geometry of the cavity in which the lung is placed during measurements. To provide more *in vivo*-like conditions during measurements, our method could be combined with innovative non-contact imaging technique and *ex vivo* lung chamber [59].

Further, while assessment of deeper, non-superficial regions of biomaterials and centrally located tissues can be desirable, the vacuum-based method can only assess stiffness near the surface of the sample that can be elongated by the vacuum pressure being applied. Modifications to the measurement system and theory would be required for precise characterization of more centrally located regions. For example, as we showed experimentally using microparticle-embedded hydrogels (Supplementary Fig. 2), the inner diameter of the capillary tube could be increased to evaluate deeper sample regions as the depth of the deformed sample measured from the surface would correlate with the cross-sectional area of surface regions exposed to vacuum pressure. In addition, feasibility of the vacuum-based method in human lungs would need to be investigated because of their thicker and more complex visceral pleural layer. In human lungs, it is possible that measured elasticity values could be mainly reflected by the stiff visceral pleura rather than the lung parenchymal tissue underneath the pleura. Further, our method is currently incapable of decoupling different force components, such as tensional force in the tissue and surface tension at the air-liquid interface within the alveoli. However, one possible way to assess the tissue stiffness in the absence of the surface tension could be filling the lung with saline solution [73]. While this fluid-filling approach could be not clinically applicable, it can allow us to evaluate lung tissue properties in certain applications, in particular donor lung regeneration [36–38,74].

The stiffness measurements demonstrated in this study are based on a key assumption that there is no-slip interaction between the probe and tissue surface [39–42]. Therefore, to reduce measurement error, it is imperative to ensure that only the tissue volume just below the tubular probe is withdrawn into the tube during measurement. Notably, we occasionally observed slipping of surrounding pleural tissue into the probe when the probe was not tightly in contact with the tissue surface. When this occurred, we detached the probe from the tissue to release the withdrawn tissue and reposition the probe onto the surface for subsequent measurements. Further, the equation used can more accurately quantify the elastic moduli of materials and tissues with homogeneous structure and linear mechanical properties. Therefore, to improve the accuracy in determining moduli of aerated hydrogels and lung parenchyma, this equation would need to be modified to accommodate the influence of the porous tissue architecture [75,76].

The measurement platform configuration described in this study was tested in intact *ex-vivo* rat lungs. In the future, a similar aspiration probe could be integrated with a flexible polymer and combined with a miniature camera or optical fiber for monitoring local tissue deformation in vivo and providing tissue stiffness values intraoperatively during open-chest surgery or video-assisted lung surgery. Further, such device can be combined with a scope (e.g., bronchoscope, endoscope, etc.) and deployed into the patients' body to evaluate tissue properties for localized and timely evaluation of pathologic tissue in situ.

5. Conclusions

The ability to determine mechanical properties of local tissue without disrupting intrinsic structure and biology can provide invaluable insights into the correlation between tissue stiffness and function. Here, we reported a non-destructive method for measuring mechanical properties in intact tissues and biomaterials. Because this method can be used to evaluate stiffness of both native tissues and biomaterials, it may be particularly useful in the design and characterization of biomimetic materials that aim to replicate mechanical properties of native tissues for use in therapeutics (e.g., tissue adhesives, sealants) or in vitro models [77,78]. Furthermore, this method could be used to evaluate acutely injured lungs, and potentially serve as a diagnostic tool for donor organ evaluation. While the current measurement system is applicable to *in-vitro* and *ex-vivo* measurements of tissues, we envision that *in-vivo* tissue characterization could be achieved with a modified configuration. Such a system could then be applied across a variety of organs and tissues to aid in diagnosis, evaluation, and treatment of injury and disease.

Supplementary Material

Refer to Web version on PubMed Central for supplementary material.

Acknowledgements

References

[1]. Butler DL, Goldstein SA, Guilak F, Functional tissue engineering: the role of biomechanics, J. Biomech. Eng. 122 (2000) 570–575. [PubMed: 11192376]

[2]. Moeendarbary E, Harris AR, Cell mechanics: principles, practices, and prospects, Wiley Interdiscip. Rev. Syst. Biol. Med. 6 (2014) 371–388. [PubMed: 25269160]

[3]. Discher DE, Mooney DJ, Zandstra PW, Growth factors, matrices, and forces combine and control stem cells, Science 324 (2009) 1673–1677. [PubMed: 19556500]

[4]. Schaffler MB, Burr DB, Stiffness of compact bone: effects of porosity and density, J. Biomech. 21 (1988) 13–16. [PubMed: 3339022]

[5]. Guimarães CF, Gasperini L, Marques AP, Reis RL, The stiffness of living tissues and its implications for tissue engineering, Nat. Rev. Mater. 5 (2020) 351–370.

[6]. Evans ND, Gentleman E, The role of material structure and mechanical properties in cell–matrix interactions, J. Mater. Chem. B 2 (2014) 2345–2356. [PubMed: 32261407]

[7]. Handorf AM, Zhou Y, Halanski MA, W.-J. Li, Tissue stiffness dictates development, homeostasis, and disease progression, Organogenesis 11 (2015) 1–15. [PubMed: 25915734]

[8]. Paszek MJ, Zahir N, Johnson KR, Lakins JN, Rozenberg GI, Gefen A, Reinhart-King CA, Margulies SS, Dembo M, Boettiger D, Tensional homeostasis and the malignant phenotype, Cancer Cell 8(2005) 241–254. [PubMed: 16169468]

[9]. Bonnans C, Chou J, Werb Z, Remodelling the extracellular matrix in development and disease, Nat. Rev. Mol. Cell Biol. 15(2014) 786–801. [PubMed: 25415508]

[10]. Lukashev ME, Werb Z, ECM signalling: orchestrating cell behaviour and misbehaviour, Trends Cell Biol. 8 (1998) 437–441. [PubMed: 9854310]

[11]. Sternlicht MD, Werb Z, How matrix metalloproteinases regulate cell behavior, Annu. Rev. Cell Dev. Biol. 17 (2001) 463–516. [PubMed: 11687497]

[12]. Lampi MC, Reinhart-King CA, Targeting extracellular matrix stiffness to attenuate disease: from molecular mechanisms to clinical trials, Sci. Transl. Med. 10 (2018).

[13]. McKee CT, Last JA, Russell P, Murphy CJ, Indentation versus tensile measurements of Young's modulus for soft biological tissues, Tissue Eng. Part B: Reviews 17 (2011) 155–164.

[14]. Bembey A, Oyen M, Bushby A, Boyde A, Viscoelastic properties of bone as a function of hydration state determined by nanoindentation, Philos. Mag. 86 (2006) 5691–5703.

[15]. Polio SR, Kundu AN, Dougan CE, Birch NP, Aurian-Blajeni DE, Schiffman JD, Crosby AJ, Peyton SR, Cross-platform mechanical characterization of lung tissue, PLoS One 13 (2018) e0204765. [PubMed: 30332434]

[16]. Veldhuizen R, Nag K, Orgeig S, Possmayer F, The role of lipids in pulmonary surfactant, Biochimica et Biophysica Acta (BBA)-Mol. Basis Dis. 1408 (1998) 90–108.

[17]. Clements JA, Hustead RF, Johnson RP, Gribetz I, Pulmonary surface tension and alveolar stability, J. Appl. Physiol. 16 (1961) 444–450. [PubMed: 13694048]

[18]. Schousboe P, Wiese L, Heiring C, Verder H, Poorisrisak P, Verder P, Nielsen HB, Assessment of pulmonary surfactant in COVID-19 patients, Critical Care 24 (2020) 1–2. [PubMed: 31898531]

[19]. Greene KE, Wright JR, Steinberg KP, Ruzinski JT, Caldwell E, Wong WB, Hull W, Whitsett JA, Akino T, Kuroki Y, Serial changes in surfactant-associated proteins in lung and serum before and after onset of ARDS, Am. J. Respir. Crit. Care Med. 160 (1999) 1843–1850. [PubMed: 10588595]

[20]. Hinz B, Mechanical aspects of lung fibrosis: a spotlight on the myofibroblast, Proc. Am. Thorac. Soc. 9 (2012) 137–147. [PubMed: 22802288]

[21]. Chen H, Qu J, Huang X, Kurundkar A, Zhu L, Yang N, Venado A, Ding Q, Liu G, Antony VB, Mechanosensing by the α 6-integrin confers an invasive fibroblast phenotype and mediates lung fibrosis, Nat. Commun. 7 (2016) 1–12.

[22]. Liu F, Tschumperlin DJ, Micro-mechanical characterization of lung tissue using atomic force microscopy, JoVE (J. Visualized Exp.) (2011) e2911.

[23]. Dietrich CF, Barr RG, Farrokh A, Dighe M, Hocke M, Jenssen C, Dong Y, Saftoiu A, Havre RF, Strain elastography-how to do it? Ultrasound Int. Open 3 (2017) E137. [PubMed: 29226273]

[24]. Taljanovic MS, Gimber LH, Becker GW, Latt LD, Klauser AS, Melville DM, Gao L, Witte RS, Shear-wave elastography: basic physics and musculoskeletal applications, Radiographics 37 (2017) 855–870. [PubMed: 28493799]

[25]. Evans A, Whelehan P, Thomson K, McLean D, Brauer K, Purdie C, Jordan L, Baker L, Thompson A, Quantitative shear wave ultrasound elastography: initial experience in solid breast masses, Breast Cancer Res. 12 (2010) 1–11.

[26]. Garra BS, Elastography: history, principles, and technique comparison, Abdom. Imaging 40 (2015) 680–697. [PubMed: 25637125]

[27]. Sigrist RM, Liau J, El Kaffas A, Chammas MC, Willmann JK, Ultrasound elastography: review of techniques and clinical applications, Theranostics 7 (2017) 1303. [PubMed: 28435467]

[28]. Hajji M, Wilson T, Lai-Fook S, Improved measurements of shear modulus and pleural membrane tension of the lung, J. Appl. Physiol. 47 (1979) 175–181. [PubMed: 468657]

[29]. Lai-Fook SJ, Pleural mechanics and fluid exchange, Physiol. Rev. 84 (2004) 385–410. [PubMed: 15044678]

[30]. Dai Z, Peng Y, Mansy HA, Sandler RH, Royston TJ, A model of lung parenchyma stress relaxation using fractional viscoelasticity, Med. Eng. Phys. 37 (2015) 752–758. [PubMed: 26050200]

[31]. Nava A, Mazza E, Furrer M, Villiger P, Reinhart W, In vivo mechanical characterization of human liver, Med. Image Anal. 12 (2008) 203–216. [PubMed: 18171633]

[32]. Dobrev H, Use of Cutometer to assess epidermal hydration, Skin Res. Technol. 6 (2000) 239–244. [PubMed: 11428963]

[33]. Evans E, New membrane concept applied to the analysis of fluid shear-and micropipette-deformed red blood cells, Biophys. J. 13 (1973) 941–954. [PubMed: 4733701]

[34]. Evans EA, Waugh R, Melnik L, Elastic area compressibility modulus of red cell membrane, Biophys. J. 16 (1976) 585–595. [PubMed: 1276386]

[35]. Kim J, O'Neill JD, Dorrello NV, Bacchetta M, Vunjak-Novakovic G, Targeted delivery of liquid microvolumes into the lung, Proc. Natl. Acad. Sci. 112 (2015) 11530–11535. [PubMed: 26324893]

[36]. O'Neill JD, Guenthart BA, Kim J, Chicotka S, Queen D, Fung K, Marboe C, Romanov A, Huang SX, Y.-.W. Chen, Cross-circulation for extracorporeal support and recovery of the lung, Nature Biomed. Eng. 1 (2017) 1–15.

[37]. Dorrello NV, Guenthart BA, O'Neill JD, Kim J, Cunningham K, Y.-.W. Chen, Biscotti M, Swayne T, Wobma HM, Huang SX, Functional vascularized lung grafts for lung bioengineering, Sci. Adv. 3 (2017) e1700521. [PubMed: 28875163]

[38]. Guenthart BA, O'Neill JD, Kim J, Queen D, Chicotka S, Fung K, Simpson M, Donocoff R, Salna M, Marboe CC, Regeneration of severely damaged lungs using an interventional cross-circulation platform, Nat. Commun. 10 (2019) 1–16. [PubMed: 30602773]

[39]. Hochmuth RM, Micropipette aspiration of living cells, J. Biomech. 33 (2000) 15–22. [PubMed: 10609514]

[40]. Sato M, Theret D, Wheeler L, Ohshima N, Nerem R, Application of the Micropipette Technique to the Measurement of Cultured Porcine Aortic Endothelial Cell Viscoelastic Properties, 1990.

[41]. Sakai A, Murayama Y, Yanagisawa M, Cyclic Micropipette Aspiration Reveals Viscoelastic Change of a Gelatin Microgel Prepared Inside a Lipid Droplet, Langmuir 36 (2020) 5186–5191. [PubMed: 32347734]

[42]. The ret D, Levesque M, Sato M, Nerem R, Wheeler L, The Application of a Homogeneous Half-Space Model in the Analysis of Endothelial Cell Micropipette Measurements, 1988.

[43]. Czerner M, Fellay LS, Suárez MP, Frontini PM, Fasce LA, Determination of elastic modulus of gelatin gels by indentation experiments, Procedia Mater. Sci. 8(2015) 287–296.

[44]. Van Den Bulcke AI, Bogdanov B, De Rooze N, Schacht EH, Cornelissen M, Berghmans H, Structural and rheological properties of methacrylamide modified gelatin hydrogels, Biomacromolecules 1 (2000) 31–38. [PubMed: 11709840]

[45]. Joly-Duhamel C, Hellio D, Ajdari A, Djabourov M, All gelatin networks: 2. the master curve for elasticity, Langmuir 18 (2002) 7158–7166.

[46]. Bou Jawde S, Takahashi A, Bates JHT, Suki B, An Analytical Model for Estimating Alveolar Wall Elastic Moduli From Lung Tissue Uniaxial Stress-Strain Curves, (in English), Front. Physiol. Original Res. (2020) 11.

[47]. Suki B, Bates JH, Lung tissue mechanics as an emergent phenomenon, J. Appl. Physiol. 110 (2011) 1111–1118. [PubMed: 21212247]

[48]. Suki B, Stamenovi D, Hubmayr R, Lung parenchymal mechanics, Compr. Physiol. 1 (2011) 1317–1351. [PubMed: 23733644]

[49]. Crapo PM, Gilbert TW, Badylak SF, An overview of tissue and whole organ decellularization processes, Biomaterials 32 (2011) 3233–3243. [PubMed: 21296410]

[50]. Matute-Bello G, Downey G, Moore B, Groshong S, Matthay M, Slutsky A, Kuebler W, Acute Lung Injury in Animals Study Group: an official American Thoracic Society workshop report: features and measurements of experimental acute lung injury in animals, Am. J. Respir. Cell Mol. Biol. 44 (2011) 725–738. [PubMed: 21531958]

[51]. Matute-Bello G, Frevert CW, Martin TR, Animal models of acute lung injury, Am. J. Physiol.-Lung Cellular Mol. Physiol. 295 (2008) L379–399. [PubMed: 18621912]

[52]. Bou Jawde S, Takahashi A, Bates JH, Suki B, An analytical model for estimating alveolar wall elastic moduli from lung tissue uniaxial stress-strain curves, Front. Physiol. 11 (2020) 121. [PubMed: 32158400]

[53]. Jorba I, Beltrán G, Falcones B, Suki B, Farré R, García-Aznar JM, Navajas D, Nonlinear elasticity of the lung extracellular microenvironment is regulated by macroscale tissue strain, Acta Biomater. 92 (2019) 265–276. [PubMed: 31085362]

[54]. Burgoyne CF, Downs JC, Bellezza AJ, Suh J-KF, Hart RT, The optic nerve head as a biomechanical structure: a new paradigm for understanding the role of IOP-related stress and strain in the pathophysiology of glaucomatous optic nerve head damage, Prog. Retin. Eye Res. 24 (2005) 39–73. [PubMed: 15555526]

[55]. Colan SD, H. C.s., From the Department of Cardiology, Mechanics of left ventricular systolic and diastolic function in physiologic hypertrophy of the athlete's heart, Cardiol.Clin. 15(1997) 355–372. [PubMed: 9276162]

[56]. Shelmerdine S, Barber J, George C, Applications of Laplace's law in clinical medicine: a radiological pictorial review, Br. J. Hosp. Med. 74 (2005) 451–456 2013.

[57]. Pham T, Brochard LJ, Slutsky AS, Mechanical ventilation: state of the art, in: Mayo Clinic Proceedings, 92, Elsevier, 2017, pp. 1382–1400. [PubMed: 28870355]

[58]. Gattinoni L, Marini JJ, Collino F, Maiolo G, Rapetti F, Tonetti T, Vasques F, Quintel M, The future of mechanical ventilation: lessons from the present and the past, Crit. Care 21 (2017) 1–11. [PubMed: 28057037]

[59]. Mariano CA, Sattari S, Maghsoudi-Ganjeh M, Tartibi M, Lo DD, Eskandari M, Novel Mechanical Strain Characterization of Ventilated ex vivo Porcine and Murine Lung using Digital Image Correlation, (in eng), Front. Physiol. 11 (2020) 600492. [PubMed: 33343395]

[60]. Eskandari M, Arvayo AL, Levenston ME, Mechanical properties of the airway tree: heterogeneous and anisotropic pseudoelastic and viscoelastic tissue responses, (in eng), J. Appl. Physiol. 125 (1985) 878–888 2018. [PubMed: 29745796]

[61]. Lai-Fook SJ, Kaplowitz MR, Pleural space thickness in situ by light microscopy in five mammalian species, (in eng), J. Appl. Physiol. 59 (1985) 603–610 1985. [PubMed: 4030613]

[62]. Hetzer S, Birr P, Fehlner A, Hirsch S, Dittmann F, Barnhill E, Braun J, Sack I, Perfusion alters stiffness of deep gray matter, (in eng), J. Cereb. Blood Flow Metab. 38 (2018) 116–125. [PubMed: 28151092]

[63]. Bohlin K, Bouhafs RK, Jarstrand C, Curstedt T, Blennow M, Robertson B, Spontaneous breathing or mechanical ventilation alters lung compliance and tissue association of exogenous surfactant in preterm newborn rabbits, Pediatr. Res. 57 (2005) 624–630. [PubMed: 15718361]

[64]. Welk B, Malloy JL, Joseph M, L.-J. Yao, Veldhuizen RA, Surfactant treatment for ventilation-induced lung injury in rats: effects on lung compliance and cytokines, Exp. Lung Res. 27 (2001) 505–520. [PubMed: 11558967]

[65]. Busani S, Dall'Ara L, Tonelli R, Clini E, Munari E, Venturelli S, Meschiari M, Guaraldi G, Cossarizza A, Ranieri VM, Surfactant replacement might help recovery of low-compliance lung in severe COVID-19 pneumonia, Ther. Adv. Respir. Dis. 14 (2020) 1753466620951043. [PubMed: 32865137]

[66]. Grossman RF, Jones JG, Murray JF, Effects of oleic acid-induced pulmonary edema on lung mechanics, J. Appl. Physiol. 48 (1980) 1045–1051. [PubMed: 7380701]

[67]. Noble W, Kay J, Obdrzalek J, Lung mechanics in hypervolemic pulmonary edema, J. Appl. Physiol. 38 (1975) 681–687. [PubMed: 1141099]

[68]. Pathak A, Kumar S, Independent regulation of tumor cell migration by matrix stiffness and confinement, Proc. Natl. Acad. Sci. 109 (2012) 10334–10339. [PubMed: 22689955]

[69]. Pathak A, Kumar S, Biophysical regulation of tumor cell invasion: moving beyond matrix stiffness, Integr. Biol. 3 (2011) 267–278.

[70]. Fang Q, Curatolo A, Wijesinghe P, Yeow YL, Hamzah J, Noble PB, Karnowski K, Sampson DD, Ganss R, Kim JK, Ultrahigh-resolution optical coherence elastography through a micro-endoscope: towards in vivo imaging of cellular-scale mechanics, Biomed. Opt. Express 8 (2017) 5127–5138. [PubMed: 29188108]

[71]. Chen MH, Wang LL, Chung JJ, Y.-.H. Kim, Atluri P, Burdick JA, Methods to assess shear-thinning hydrogels for application as injectable biomaterials, ACS Biomater. Sci. Eng. 3 (2017) 3146–3160. [PubMed: 29250593]

[72]. Eftimov PB, Yokoi N, Peev N, Paunski Y, Georgiev GA, Relationships between the material properties of silicone hydrogels: desiccation, wettability and lubricity, J. Biomater. Appl. (2020) 0885328220967526.

[73]. Mitzner W, Mechanics of the lung in the 20th century, Compr. Physiol. 1 (2011) 2009–2027. [PubMed: 23733695]

[74]. Kim J, Guenthart B, O'Neill JD, Dorrello NV, Bacchetta M, Vunjak-No-vakovic G, Controlled delivery and minimally invasive imaging of stem cells in the lung, Sci. Rep. 7 (2017) 1–13. [PubMed: 28127051]

[75]. Ková ik J, Correlation between Young's modulus and porosity in porous materials, J. Mater. Sci. Lett. 18 (1999) 1007–1010.

[76]. Wang JC, Young's modulus of porous materials, J. Mater. Sci. 19 (1984) 801–808.

[77]. Vining KH, Mooney DJ, Mechanical forces direct stem cell behaviour in development and regeneration, Nat. Rev. Mol. Cell Biol. 18 (2017) 728–742. [PubMed: 29115301]

[78]. Chaudhuri O, Cooper-White J, Janmey PA, Mooney DJ, Shenoy VB, Effects of extracellular matrix viscoelasticity on cellular behaviour, Nature 584 (2020) 535–546. [PubMed: 32848221]

Author Manuscript

Author Manuscript

Author Manuscript

Author Manuscript

Statement of significance

Accurate quantification of tissue stiffness is critical for understanding mechanisms of disease and developing effective therapeutics. Current modalities to measure tissue stiffness are destructive and preclude accurate assessment of lung mechanical properties, as lung mechanics are determined by complex features of the intact lung. To address the need for alternative methods to assess lung mechanics, we report a non-destructive vacuum-based approach to quantify tissue stiffness. We applied this method to correlate lung tissue mechanics with tissue disruption, and to assess the stiffness of biomaterials. This method can be used to inform the development of tissue-mimetic materials for use in therapeutics and disease models, and could potentially be applied for *in-situ* evaluation of tissue stiffness as a diagnostic or prognostic tool.
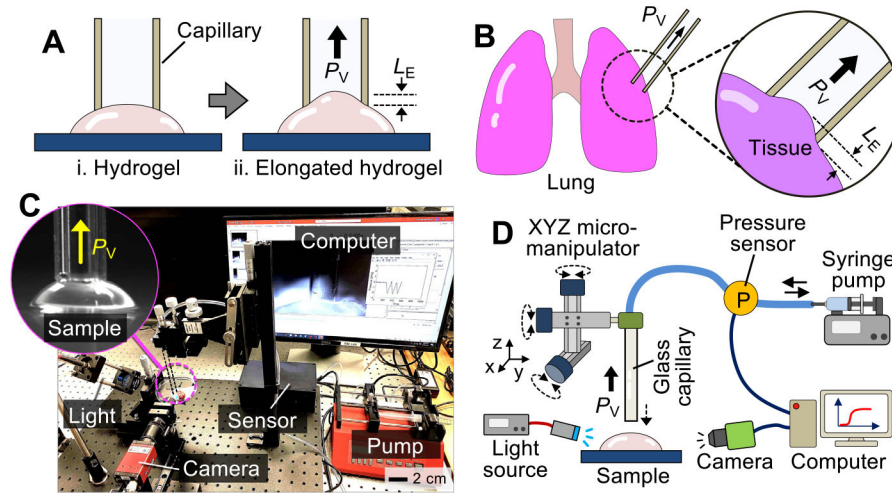
Fig. 1. Overview of vacuum-based measurement of elastic moduli of soft biomaterials, including hydrogels and tissues:

Schematic of (**A**) hydrogel and (**B**) lung tissue deformed via vacuum pressure. P_V: vacuum pressure. L_E: elongation length. (**C**) Custom-built system to measure the stiffness of soft biomaterials and *ex vivo* lung. (**D**) Schematic of measurement system. P: Air pressure sensor.
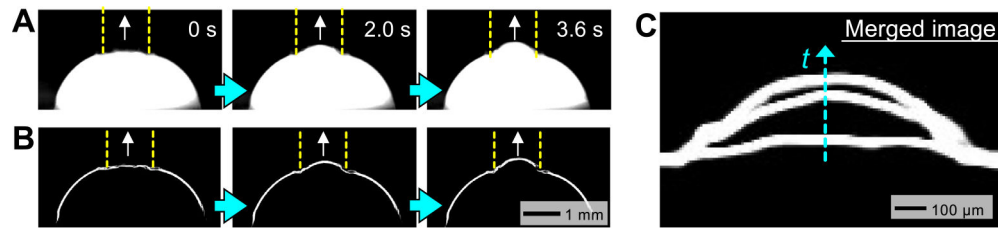
Fig. 2. Gelatin hydrogel (4%w/v) used to evaluate functionality of the measurement system:
(**A**) Stiffness measurement was demonstrated using a dome-shaped 4% w/v gelatin hydrogel formed on a PDMS substrate. To enhance visibility of gel deformation, fluorescein dye was added to the gelatin. (**B**) Via edge detection, the deformed shape of the gelatin was determined. (**C**) Merged image of the deformed region of the gelatin showing elongation of the gel due to vacuum pressure over time.
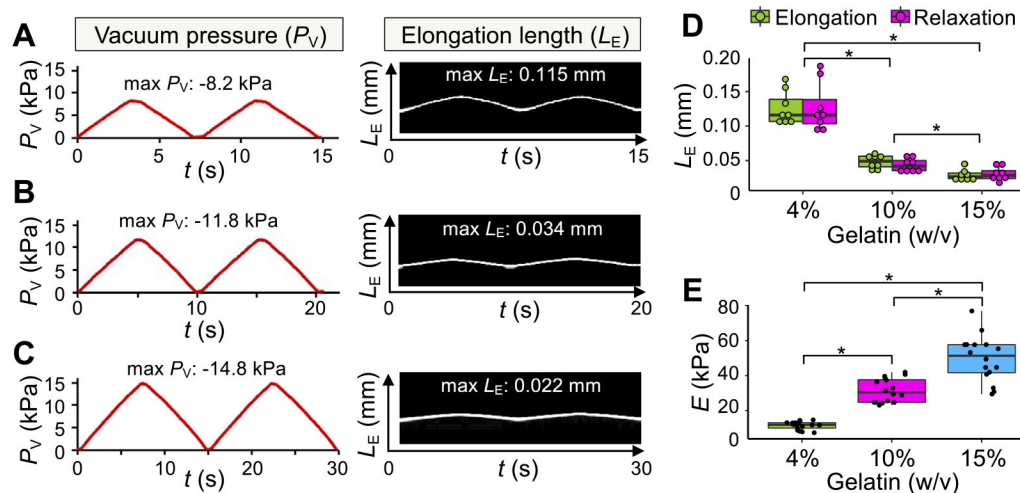
Fig. 3. Cyclic vacuum-loading on gelatin hydrogels of different concentrations:
Applied negative pressure (P_V) and measured elongation length (L_E) are plotted for (**A**) 4%, (**B**) 10%, and (**C**) 15% w/v gelatin. For all samples, the rate of negative pressure increased or decreased (i.e., slope of aspiration curve) was approximately 2.25 kPa/s. (**D**) Elongation length (L_E) of the gelatin under P_V of −5 kPa was determined during elongation and relaxation period of the gel, respectively. (**E**) Elastic modulus (E) of each gelatin hydrogel was determined based on the measurement condition. All values represent mean ± standard deviation. $*p < 0.001$.
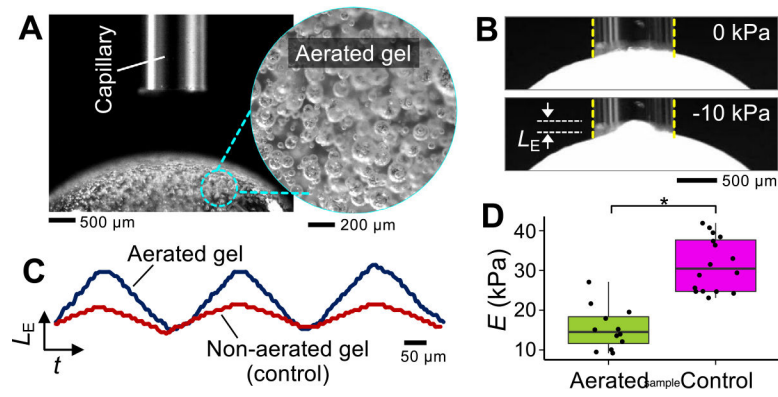
Fig. 4. Effects of porosity on gelatin deformation mechanics:
(**A**) Aerated 10% w/v gelatin was tested to investigate the correlation between gel porosity and stiffness. (**B**) Images of the aerated gel showing deformed shape under vacuum pressure (P_V) of −10 kPa. (**C**) Deformation of both aerated and non-aerated (control) 10% w/v gelatin under cyclic vacuum pressure loading over time. (**D**) Elastic modulus (E) of the aerated and non-aerated 10% w/v gelatin. All values represent mean ± standard deviation. *$p < 0.001$.
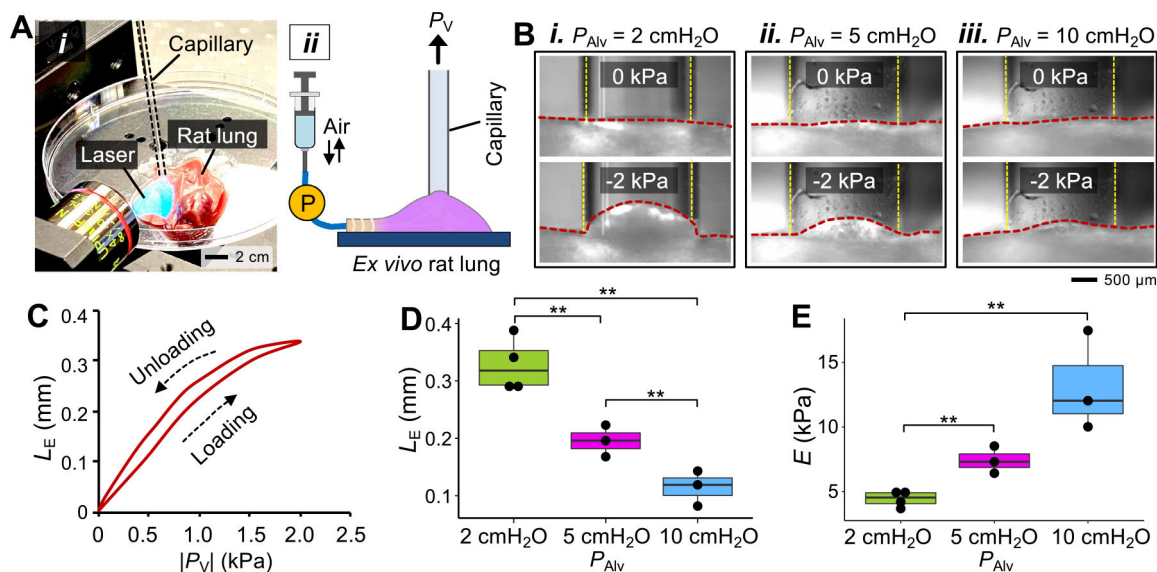
Fig. 5. Deformation behavior of *ex vivo* rat lungs:
(**A**) (*i*) Photograph and (*ii*) schematic of setup for measuring stiffness of *ex vivo* rat lung.
P: air pressure sensor. (**B**) Lung tissue was subjected to vacuum pressure of −2 kPa via a
glass capillary tube (inner diameter: 1.5 mm) while the intra-alveolar pressure (P_{ALV}) was
maintained at different pressure levels: (*i*) 2 cmH_2O, (*ii*) 5 cmH_2O, (*iii*) 10 cmH_2O. (**C**)
Elongation length (L_E) measured while varying magnitude of vacuum pressure ($|P_V|$). (**D**)
Maximum elongation length (L_E) and (**E**) elastic modulus (E) of lung tissue against different
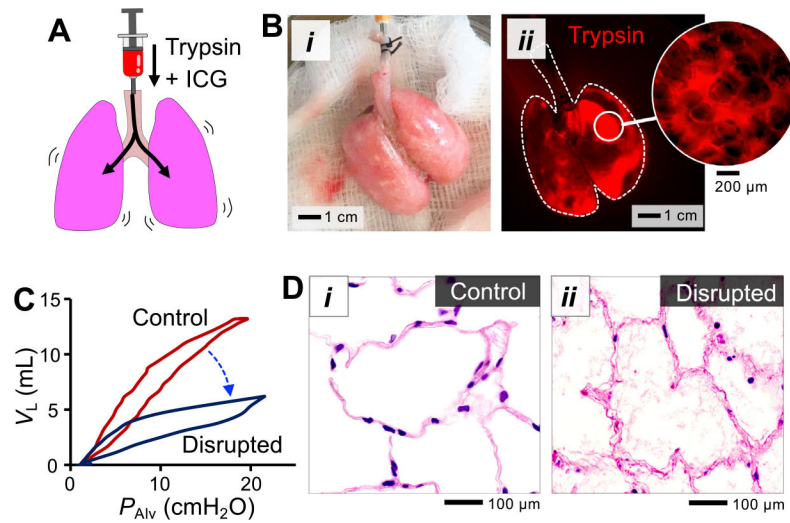P_{Alv}. **$p < 0.05$.

Fig. 6. Effects of enzymatic tissue disruption on lung deformation mechanics:
(**A**) Schematic of lung tissue disruption induced by intratracheal instillation of trypsin with ICG fluorescent dye. (**B**) (*i*) Explanted rat lungs before trypsin challenge. (*ii*) Distribution of trypsin/ICG (red) in alveolar space visualized via NIR imaging. (**C**) Pressure-volume (PV) curves of the lung before and after trypsinization were obtained by measuring the intra-alveolar pressure (P_{Alv}) and volume (V_L) of air inspired or expired through the trachea of the lung using a small animal ventilator. (**D**) H&E images of the alveoli of (*i*) control (healthy) and (*ii*) enzymatically disrupted rat lungs.
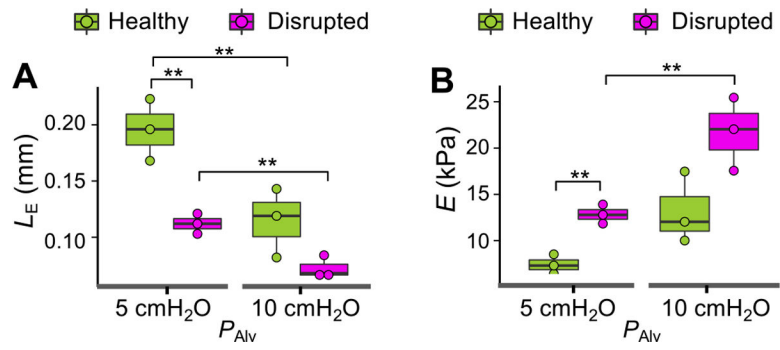
Fig. 7. Alteration in elastic moduli of enzymatically disrupted lung parenchyma:
(**A**) Maximum elongation length (L_E) and (**B**) elastic modulus (E) of lungs were determined under different P_{Alv} for both control (healthy) and trypsin challenged (disrupted) lungs. All values represent mean ± standard deviation. $**p < 0.05$.